The Astronomical Journal, 132:1998–2013, 2006 November

SUBMILLIMETER COMMON-USER BOLOMETER ARRAY MAPPING OF *SPITZER* c2d SMALL CLOUDS AND CORES

Chadwick H. Young
Department of Physical Sciences, Nicholls State University, P.O. Box 2022, Thibodaux, LA 70301

Tyler L. Bourke
Harvard-Smithsonian Center for Astrophysics, 60 Garden Street, Cambridge, MA 02138

Kaisa E. Young
Department of Physical Sciences, Nicholls State University, P.O. Box 2022, Thibodaux, LA 70301

Neal J. Evans II
Department of Astronomy, University of Texas at Austin, Austin, TX 78712-1083

Jes K. Jørgensen
Harvard-Smithsonian Center for Astrophysics, 60 Garden Street, Cambridge, MA 02138

Yancy L. Shirley
Steward Observatory, University of Arizona, Tucson, AZ 85721

and

Ewine F. van Dishoeck and Michiel Hogerheijde
Leiden Observatory, P.O. Box 9513, 2300 RA Leiden, Netherlands
Received 2006 May 16; accepted 2006 June 28

ABSTRACT

We present submillimeter observations of dark clouds that are part of the *Spitzer* Legacy program "From Molecular Cores to Planet-Forming Disks" (c2d). We used the Submillimeter Common-User Bolometer Array to map the regions observed by *Spitzer* with the c2d program to create a census of dense molecular cores including data from the infrared to the submillimeter. In this paper we present the basic data from these observations: maps, fluxes, and source attributes. We also show data for an object just outside the Perseus cloud that was serendipitously observed in our program. We propose that this object is a newly discovered evolved protostar.

Key words: stars: formation — stars: low-mass, brown dwarfs — stars: pre–main-sequence

1. INTRODUCTION

In recent years, significant progress has been made toward a theory for the formation of low-mass stars, which are the likely sites of formation of planetary systems. Maps of submillimeter dust continuum emission are excellent tracers of the column density and mass. Dust continuum emission has been used to map both large clouds (e.g., Motte et al. 1998; Johnstone et al. 2004; Enoch et al. 2006) and smaller cores (e.g., Shirley et al. 2000; Visser et al. 2002; Young et al. 2003; Kirk et al. 2005).

Studies of small cores provide complementary advantages to less biased surveys of large clouds. By focusing on regions already known to have dense gas, we can study their properties in more detail. The large-scale surveys can, in turn, check the biases that are introduced. This paper presents data on dust continuum emission toward a large number of small cores.

For a full analysis, data at submillimeter wavelengths should be combined with data through the infrared. The *Spitzer* Legacy program "From Molecular Cores to Planet-Forming Disks" (c2d), described by Evans et al. (2003), has obtained extremely sensitive observations from 3.6 to 70 μm toward 105 small cores (T. L. Huard et al. 2006, in preparation). In order to obtain the full benefit of this database, it is crucial to add data at longer wavelengths, where the dust emission is optically thin.

We have mapped 38 small cores, which were initially included in the c2d program, using the Submillimeter Common-User Bolometer Array (SCUBA) at both 850 and 450 μm. Because of time constraints, 15 of these cores were dropped from the c2d program, although some were covered by the large cloud map of Perseus (Jørgensen et al. 2006; L. Rebull et al. 2006, in preparation). Together with other complementary data at optical and near-infrared wavelengths, our observations provide a comprehensive catalog of multiwavelength data for a sample of small molecular cores. The goal of this paper is to present the SCUBA[1] data in a uniform way, consistent with other papers presenting submillimeter continuum data on the c2d cores and clouds.We leave detailed analysis to later papers that combine these data with the c2d data.

2. OBSERVATIONS AND DATA REDUCTION

2.1. *Sample*

The sample was drawn from those cores originally included in the c2d observation plan. In turn, those cores had been drawn from catalogs of nearby cores that have molecular line maps (Lee & Myers 1999; Jijina et al. 1999; Lee et al. 2001). The gas in these cores is well studied, mostly by mapping observations of the 1.3 cm line of NH_3 (Benson & Myers 1989) and the 3 mm line of N_2H^+ (Caselli et al. 2002). These cores are all relatively nearby, within 450 pc, so their maps have good spatial resolution. A few cores have been observed in the submillimeter before, but not over a region as large as that mapped by the *Spitzer Space*

[1] The data are publicly available at http://peggysue.as.utexas.edu/SIRTF/DATA/.

TABLE 1
SOURCES

Source Name	R.A. (J2000.0)	Decl. (J2000.0)	Association	Dist. (pc)	Ref.	*IRAS*[a] (Y/N)	SCUBA (Y/N)	*Spitzer*[b] (Y/N)	3 σ (850 μm) (mJy beam^{-1})	3 σ (450 μm) (mJy beam^{-1})	τ_{850}	τ_{450}
Per 4B	03 29 17.9	31 27 31	Perseus	250	1	NNY	YYY	P	220	2500	0.4	2.4
Per 5	03 29 51.6	31 39 04	Perseus	250	1	Y	Y	P	190	3900	0.44	3.0
Per 6	03 30 14.9	30 23 49	Perseus	250	1	Y	Y	P	150	6500	0.44	3.0
2MASS 0347392	03 47 37.6	31 19 27	Perseus	250	1	N	Y	N	110	4200	0.49	3.2
IRAM 04191+1522	04 21 56.9	15 29 47	Taurus	140	2	NY	YY	Y	120	800	0.26	1.3
L1521F	04 28 39.8	26 51 35	Taurus	140	2	N	Y	Y	190	3100	0.29	1.6
L1524-4	04 30 05.7	24 25 16	Taurus	140	2	N	Y	Y	200	1700	0.39	1.7
B18-1	04 31 57.7	24 32 30	Taurus	140	2	N	Y	Y	190	5900	0.44	2.7
IRAS 04361+2547	04 39 13.9	25 53 21	Taurus	140	2	Y	Y	N	180	8600	0.44	3.0
RNO 43	05 32 27.9	12 53 11	...	400	3	Y	Y	N	170	1800	0.22	1.2
B35A	05 44 37.0	09 10 13	...	400	3	Y	Y	Y	220	2000	0.19	0.9
L43	16 34 30.2	−15 46 56	Ophiuchus	125	4	YN	YY	Y	240	2700	0.27	1.5
CB 68	16 57 20.5	−16 09 02	Ophiuchus	125	4	Y	Y	Y	370	4100	0.29	1.3
L492	18 15 49.0	−03 45 30	...	270	5	N	Y	Y	120	500	0.15	0.6
L723	19 17 53.2	19 12 17	...	300	6	Y	Y	Y	190	1400	0.24	1.2
L1152	20 35 46.0	67 52 42	...	325	7	Y	Y	Y	350	2700	0.2	0.9
CB 224	20 36 20.3	63 52 55	...	400	8	Y	Y	N	120	1000	0.19	1.0
L1157	20 39 06.2	68 02 42	...	325	7	YN	YY	N	160	1100	0.16	0.7
L1082C	20 51 27.6	60 18 35	...	400	8	Y	Y	N	140	2500	0.34	2.1
L1082A	20 53 34.0	60 13 41	...	400	8	YYN	YYY	N	160	1400	0.22	1.1
L1228	20 57 11.8	77 35 48	...	200	9	Y	Y	Y	350	5900	0.26	1.5
L1177 (CB 230)	21 17 43.0	68 18 24	...	288	7	Y	Y	N	180	1600	0.26	1.2
L1221	22 28 03.0	69 01 12	...	250	10	YN	YY	Y	160	2400	0.31	1.8
L1251C	22 35 24.0	75 17 09	...	300	11	Y	Y	Y	330	4800	0.26	1.5
L1251E	22 38 20.7	75 11 03	...	300	11	YNYN	YYYY	Y	260	5300	0.29	1.6
Per 7A	03 32 26.6	30 59 57	Perseus	250	1	Y	N	P	200	1800	0.37	2.2
Per 7B	03 33 15.3	30 59 54	Perseus	250	1	N	N	P	140	1500	0.35	2.1
L1521B-2	04 23 37.0	26 40 06	Taurus	140	2	N	N	Y	190	2300	0.4	2.4
L1521-2	04 29 31.8	26 59 59	Taurus	140	2	N	N	Y	260	1600	0.39	1.7
B18-5	04 35 53.0	24 09 32	Taurus	140	2	N	N	Y	180	9500	0.51	3.8
TMC 1-2	04 41 10.0	25 49 28	Taurus	140	2	Y	N	Y	320	4800	0.55	2.7
TMC 1-1	04 41 44.0	25 42 22	Taurus	140	2	N	N	Y	190	24900	0.38	2.9
CB 28	05 06 16.0	−03 56 29	...	450	12	Y	N	N	350	6400	0.25	1.7
DCld 253.6+02.9	08 28 44.0	−33 45 12	...	450	13	Y	N	N	330	7400	0.22	1.2
L1772	17 19 32.7	−26 44 40	Ophiuchus	125	4	N	N	Y	260	2900	0.26	1.5
L55	17 22 58.0	−23 57 18	Ophiuchus	125	4	N	N	N	280	3100	0.25	1.2
B72	17 23 46.3	−23 41 20	Ophiuchus	125	4	N	N	Y	340	4100	0.32	1.9
L1155C	20 43 06.0	67 49 56	...	325	7	Y	N	Y	210	1700	0.21	1.0

NOTE.— Units of right ascension are hours, minutes, and seconds, and units of declination are degrees, arcminutes, and arcseconds.

[a] We search a 1′ radius for detections by *IRAS*. The *IRAS* sources must meet the criteria presented by Lee & Myers (1999). More than one symbol implies that more than one submillimeter core was found.

[b] A "Y" means that the core was observed by *Spitzer* as part of the c2d cores program, an "N" means that it was in the original cores program but was cut, and a "P" means that it was observed as part of the Perseus cloud map.

REFERENCES.— (1) Enoch et al. 2006; (2) Elias 1978; (3) Murdin & Penston 1977; (4) de Geus et al. 1989; (5) Straizys et al. 2003; (6) Goldsmith et al. 1984; (7) Straizys et al. 1992; (8) Dobashi et al. 1994; (9) Kun 1998; (10) Yonekura et al. 1997; (11) Kun & Prusti 1993; (12) Ogura & Sugitani 1998; (13) Woermann et al. 2001.

Telescope. In these observations, we have matched the SCUBA maps to cover the same area as the *Spitzer* maps; in most cases, these maps are 5′×5′, but they are sometimes larger.

Table 1 lists the central right ascension and declination for each region observed with SCUBA. This table also has the core's associated cloud, if relevant, and the distance, using the standard distances adopted for the c2d project (T. L. Huard et al. 2006, in preparation). We note whether submillimeter emission was detected in our observations (Y or N). For those with a submillimeter detection, we list whether the submillimeter core has an *IRAS* detection (within 1′ of the submillimeter peak); these *IRAS* sources were chosen based on the criteria given by Lee & Myers (1999). We also list whether there was an *IRAS* source in those maps with no detected submillimeter emission. For maps with more than one clearly separated source, we give multiple entries in the *IRAS* and SCUBA columns (e.g., YNY). Next, we indicate whether the core was observed in the cores part of the c2d program (Y) or covered by the Perseus cloud map (P). Table 1 includes the 3 σ limit for each map at both 850 and 450 μm, followed by the atmospheric opacity during the observations, again at both wavelengths. Because the goal of this project was to cover the same observed area as in the c2d program, we often observed in weather conditions that were inadequate for good 450 μm maps. This allowed us to create large maps, but the quality of the 450 μm data, as a result, is not sufficient to analyze dust temperature, emissivity, etc.

We had intended to observe Per 9, whose position is in Caselli et al. (2002). However, we improperly entered the coordinates at the telescope and mistakenly observed a field that happens to be centered on 2MASS 0347392+311912. This field is about 30″

TABLE 2
CALIBRATORS

Date	Calibrator	τ_{850}	τ_{450}	C_{20}^{850}[a]	C_{40}^{850}	C_{80}^{850}	C_{120}^{850}	C_{20}^{450}	C_{40}^{450}	C_{80}^{450}	C_{120}^{450}	FWHM[b] (arcsec)
2002 Jan 11	CRL 618	0.26	1.31	79.0	41.4	31.5	24.6	38.3	22.2	10.5	6.0	15.3
2002 Jan 11	Uranus	0.20	0.96	62.0	44.0	41.5	42.0	35.1	29.5	28.7	33.8	15.6
2002 Jan 15	CRL 618	0.40	2.37	61.8	41.5	31.9	25.0	23.6	12.6	5.6	3.1	15.5
2002 Jan 15	Mars	0.35	2.14	62.8	47.3	43.6	42.9	34.2	25.9	21.5	19.8	15.0
2002 Jan 15	Uranus	0.37	2.17	68.1	47.7	45.3	46.6	31.9	32.0	119.2	−21.5	15.9
2002 Jan 17	CRL 618	0.51	3.84	57.5	43.8	41.9	43.3	12.4	10.7	10.0	9.8	15.5
2002 Jan 17	CRL 618	0.44	3.03	76.9	47.8	43.6	42.5	24.4	15.9	7.8	5.5	15.8
2002 Jan 17	Mars	0.52	3.24	80.6	49.6	45.1	43.9	29.5	21.8	17.1	15.3	15.5
2002 Jan 18	CRL 618	0.60	4.28	76.6	38.9	27.1	19.8	5.8	2.3	0.9	0.4	16.6
2002 Jan 18	CRL 618	0.60	4.28	67.0	48.0	47.9	55.5	16.6	17.7	−8.4	−2.6	15.4
2002 Jan 18	Mars	0.55	2.69	72.0	49.3	43.1	41.0	66.3	46.5	36.0	31.4	15.5
2002 Oct 29	Jupiter[c]	0.25	1.34	155.8	68.3	50.4	48.8	198.6	68.7	49.6	47.0	...
2002 Oct 29	Uranus	0.28	1.50	71.2	55.1	52.6	53.5	74.4	64.8	89.2	917.1	15.7
2003 Mar 23	IRC 10216[c]	0.18	0.97	54.6	30.9	25.4	26.2	...	...	...	...	...
2003 Mar 23	IRC 10216	0.17	0.88	52.6	29.4	24.0	24.6	...	...	...	...	...
2003 Mar 25	IRC 10216	0.33	1.94	48.5	25.6	16.6	12.8	...	...	...	...	...
2003 Mar 26	IRC 10216	0.35	2.11	50.9	28.8	26.2	27.8	...	...	...	...	...
2003 Mar 26	Mars	0.25	1.45	61.7	42.3	39.0	38.7	54.6	40.9	36.4	36.5	15.5
2003 Mar 27	IRC 10216	0.30	1.57	54.0	29.8	23.6	22.5	...	...	...	...	...
2003 Mar 28	IRC 10216	0.20	0.87	45.1	24.6	17.7	15.0	...	...	...	...	...
2003 May 20	Uranus	0.19	0.96	48.4	37.8	35.4	35.4	35.7	28.6	26.0	26.1	14.4
2003 May 20	Uranus	0.16	0.72	56.2	39.8	37.8	37.5	50.2	38.7	33.8	34.3	15.4
2003 May 22	Uranus	0.22	1.07	56.8	38.9	34.6	34.1	41.7	28.4	24.7	23.8	16.0
2003 May 23	Uranus	0.24	1.22	52.4	40.0	37.3	36.8	51.0	41.6	37.1	35.6	15.3
2003 May 27	Uranus	0.37	2.55	53.0	40.4	37.7	37.1	25.2	20.0	17.6	17.3	15.1
Average values (standard deviation)	...	...	...	65 (10)	44 (5)	40 (6)	39 (9)	36 (18)	28 (15)	28 (31)	...	15.5 (0.5)

[a] The calibration factor, in Jy V^{-1}, for a 40″ aperture. Also, we show the 80″ and 120″ calibration factors.
[b] We give the FWHM of the beam at 850 μm. We deconvolve the measured beam size for the planet diameter; Uranus and Mars have semidiameters of 1.″72 and 3.″67, respectively.
[c] We do not include Jupiter or IRC 10216 in the average calibration factor.

from the edge of the c2d coverage for the Perseus cloud. We discuss the nature of this object in § 4.

2.2. *Observations*

We observed these cores with the 15 m James Clerk Maxwell Telescope (JCMT) beginning in 2002 January and ending in 2004 February. We were granted time during each semester between these dates. However, the data collected during semester 02A and 2002 December to 2003 February were not usable because of technical problems with the JCMT. The program identification designations for our observations are as follows: M/01B/N13, M/02A/N18, M/02B/N04, M/03A/N08, and M/03B/N10.

We used the scan-mapping technique (Holland et al. 1999), which is used to map regions much larger than SCUBA's field of view. Through this method, the telescope scans across the field while chopping by 30″, 44″, and 68″ in the scan direction, which is in the direction of both right ascension and declination. The chopping removes sky variations and DC offsets, and it creates a difference map of the source, a positive and negative source separated by the chop throw, that must be restored by software.

During the course of the observations, we measured τ_{850} and τ_{450} with frequent sky dips, compared these data with $\tau_{\rm CSO}$, and found good agreement. Finally, we observed several cores for flux calibration: CRL 618, Mars, Uranus, and IRC 10216. We generally observed at least two to three calibrators during an observing shift.

2.3. *Data Reduction*

We analyzed and reduced our data with the SCUBA User Reduction Facility (SURF; Jenness & Lightfoot 1997); we also closely followed the reduction methods of Pierce-Price (2002). Our reduction entailed flat-fielding, extinction correction, removal of bad pixels, removal of baselines, and the co-adding and rebinning of the maps.

To correct the data for atmospheric extinction, we measured τ_{850} and τ_{450} from sky dips that were completed at the time of each map; these values of τ are listed in Table 1 and Table 2 for the cores and calibrators, respectively.

For the removal of bad pixels, we first used SURF's *despike2* tool, which removes spikes from scan-map observations. This package has two criteria for despiking. The first considers each data point and asks how disparate it is from the two adjacent data points. If this difference is greater than a certain number of standard deviations for the scan (NSIGMA), the data point is rejected. We used NSIGMA=4. The second criterion convolves the data with a three-sample box and uses NSIGMA in the same way. In addition, we used *sclean* to interactively search all of the data for bad pixels.

We used SURF's *scan_rlb* to remove the baselines from the extinction-corrected and cleaned data. We assumed that there was no emission at the end of each scan, which was generally true, and used the linear method of baseline removal. In this way, *scan_rlb* fits the baseline to the end of each scan and then applies it to the remaining scan.

Next, we rebinned the data with baselines removed to create the dual-beam map. We used pixels appropriate for Nyquist sampling (3.″5 and 7.″5 for 450 and 850 μm, respectively) and did not smooth the maps; smoothing of the maps often causes artifacts from the data reduction to appear as real emission (greater than

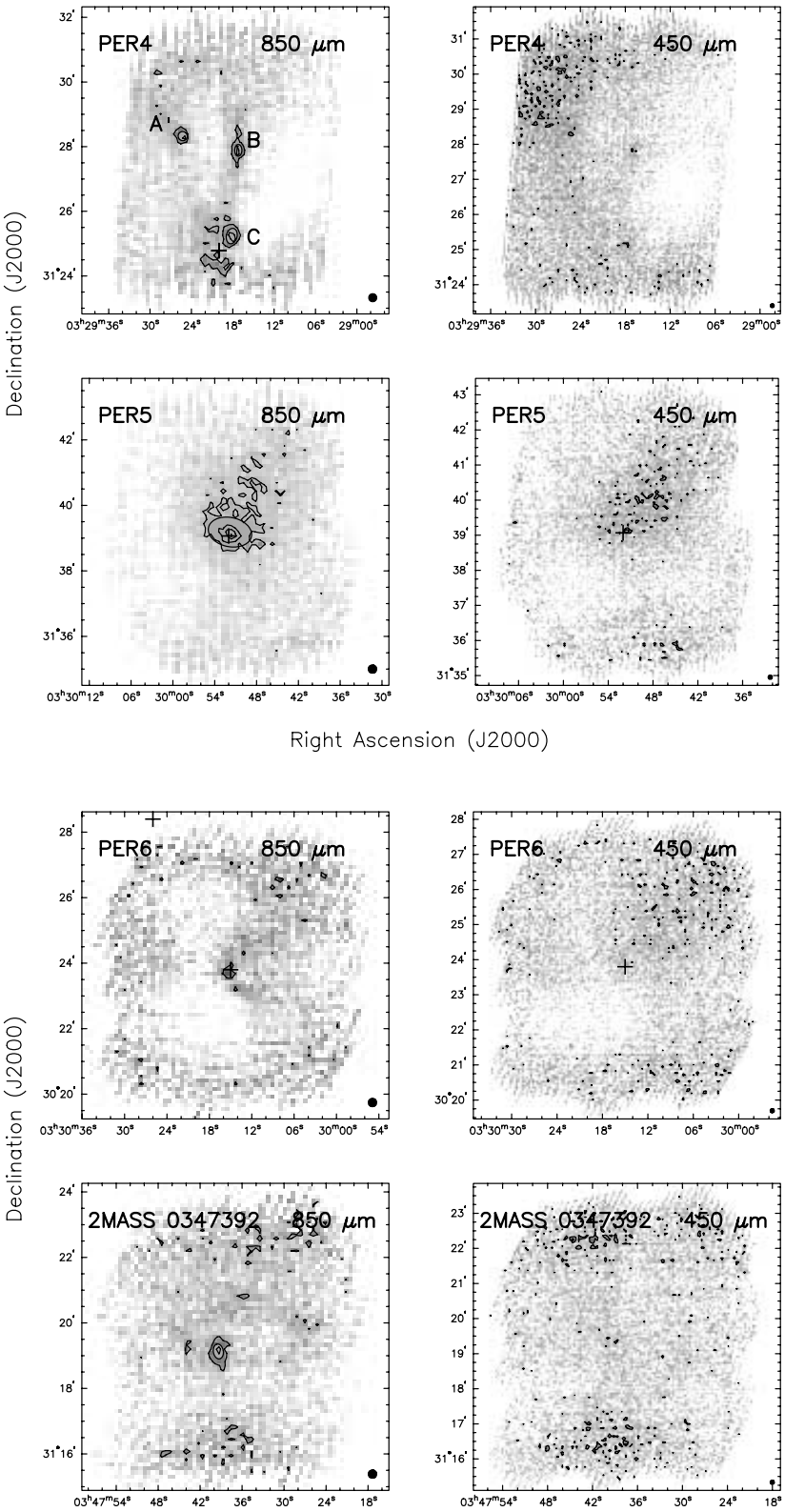

FIG. 1.—The 850 and 450 μm maps for the cores in Table 1. Contours begin at 2 σ and increase by 2 σ; gray scale begins at -2 σ and increases to the image maximum. Crosses mark the positions of *IRAS* sources in the field. The ellipses show the size and shape of the source as determined by Extractor, described in § 2.3.

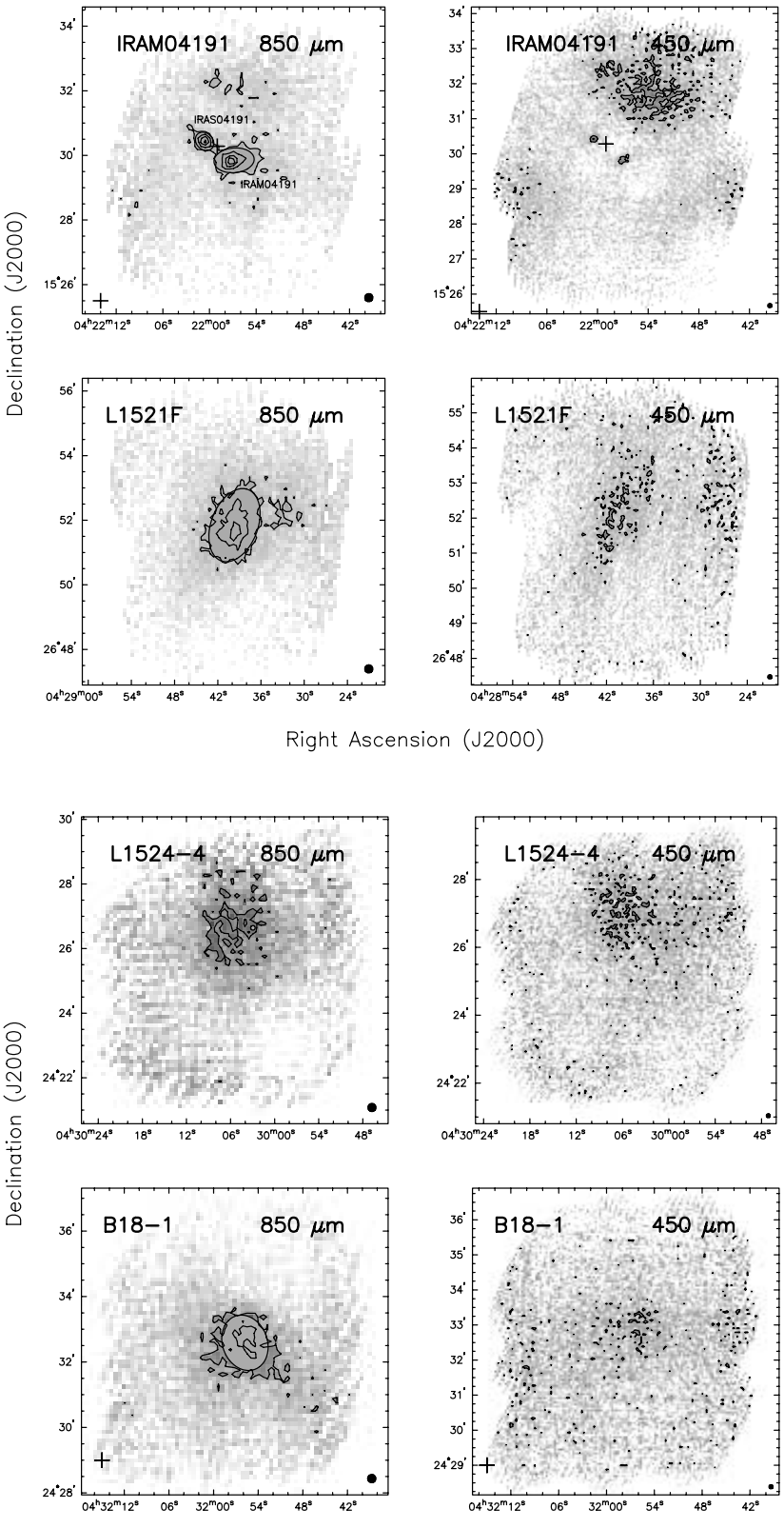

FIG. 1.—*Continued*

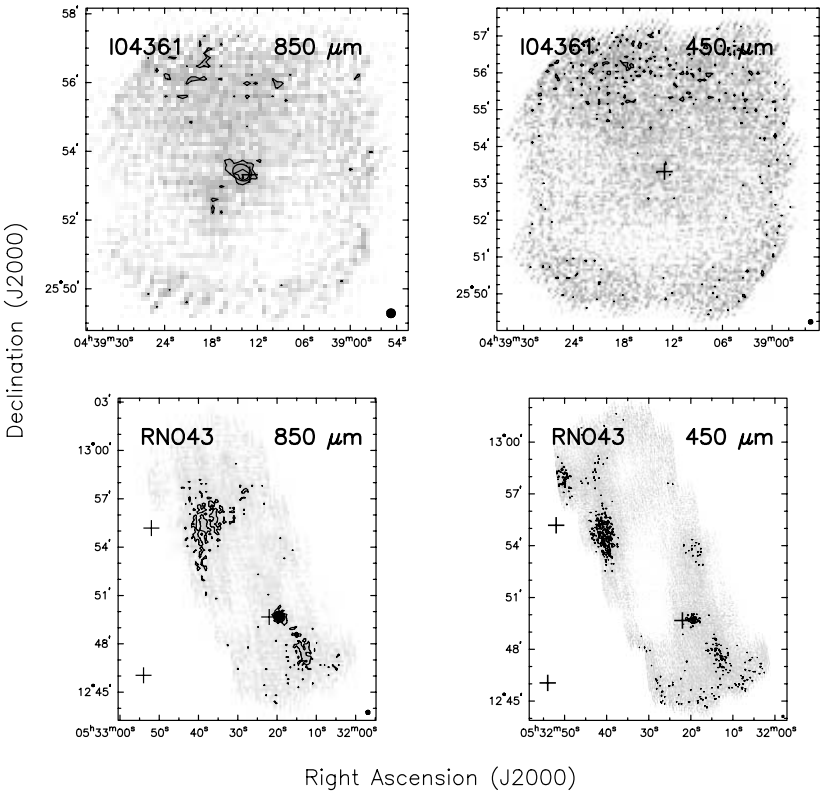

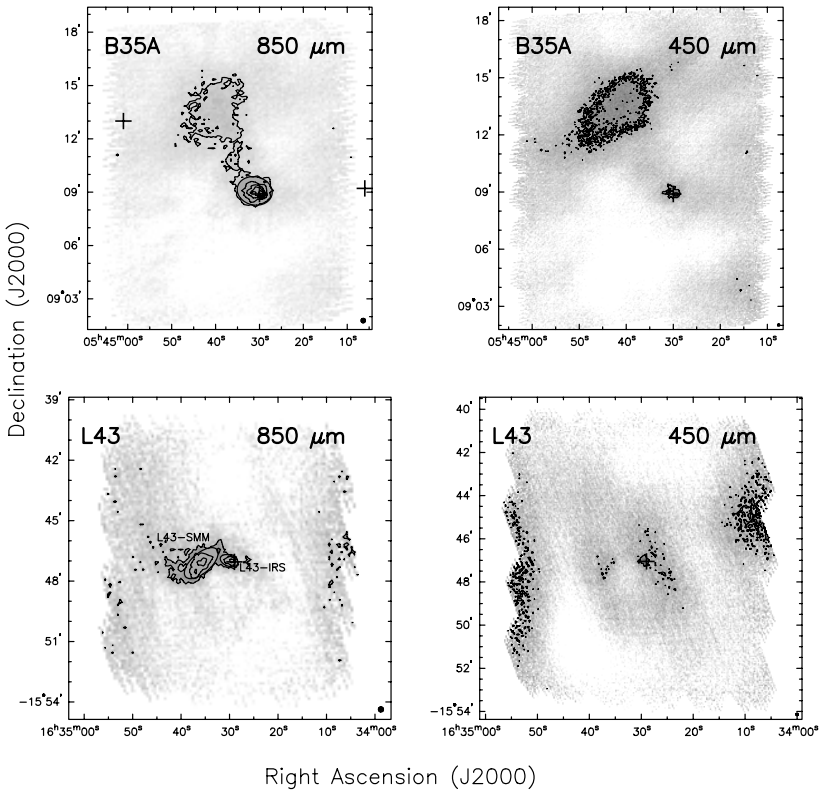

FIG. 1.—*Continued*

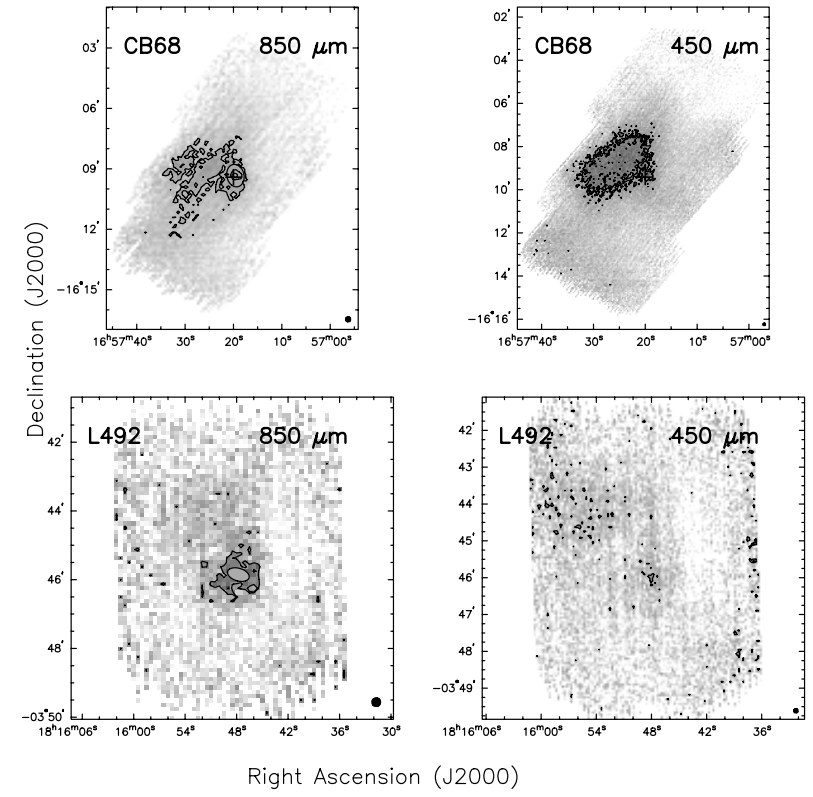

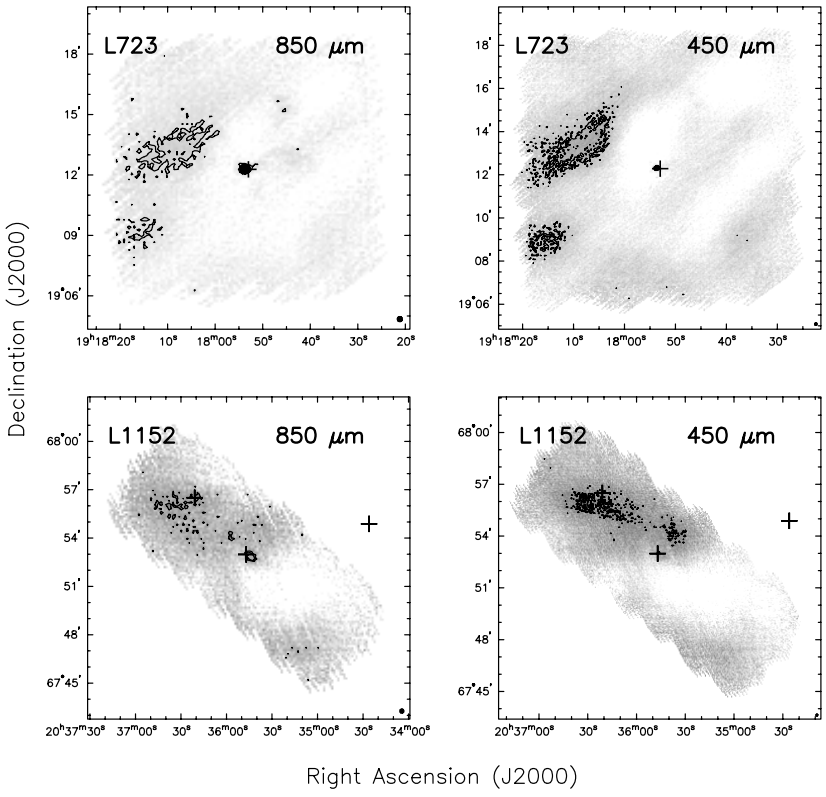

FIG. 1.—*Continued*

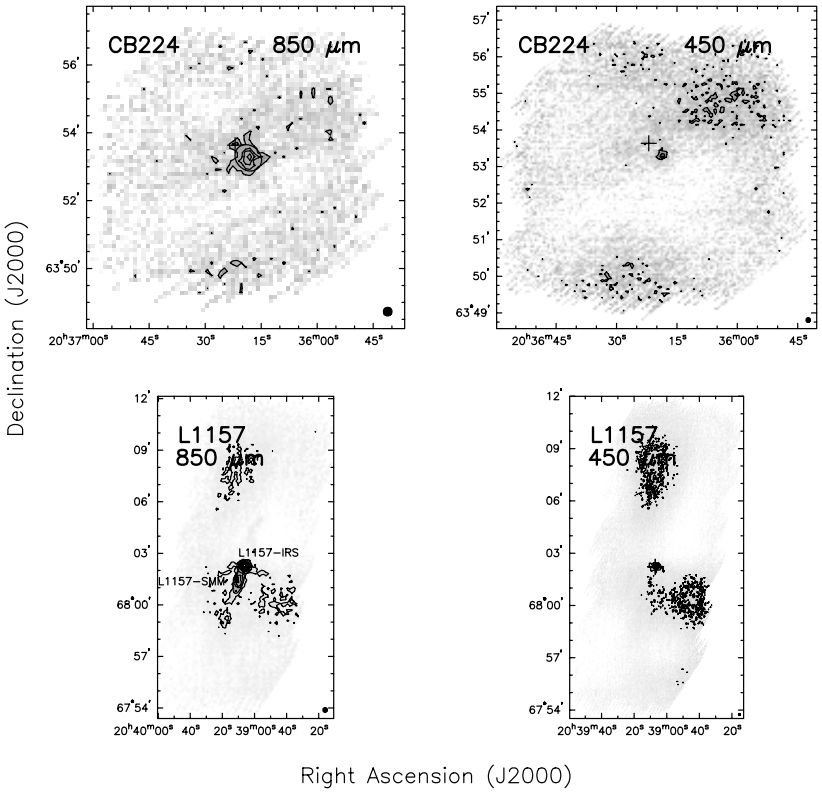

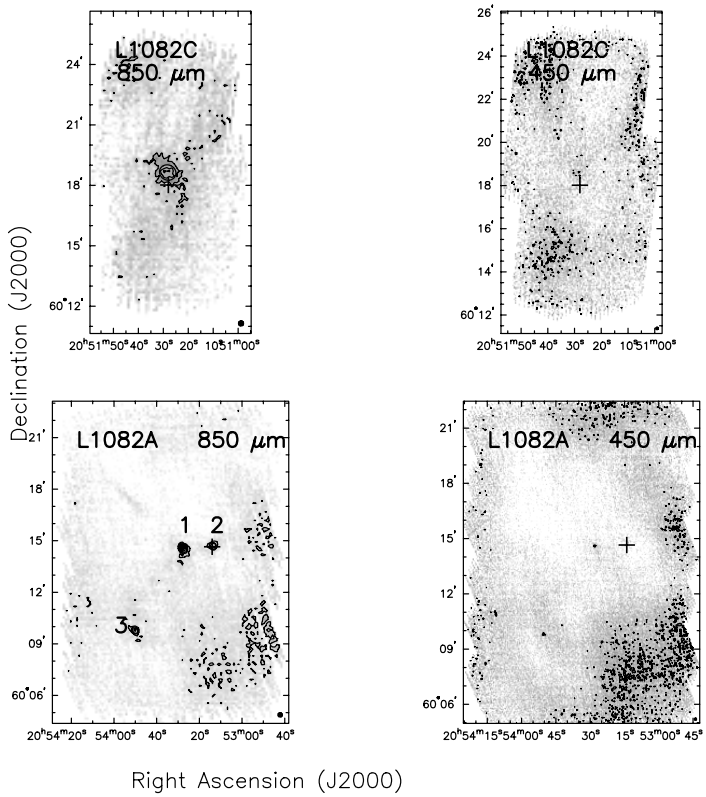

FIG. 1.—*Continued*

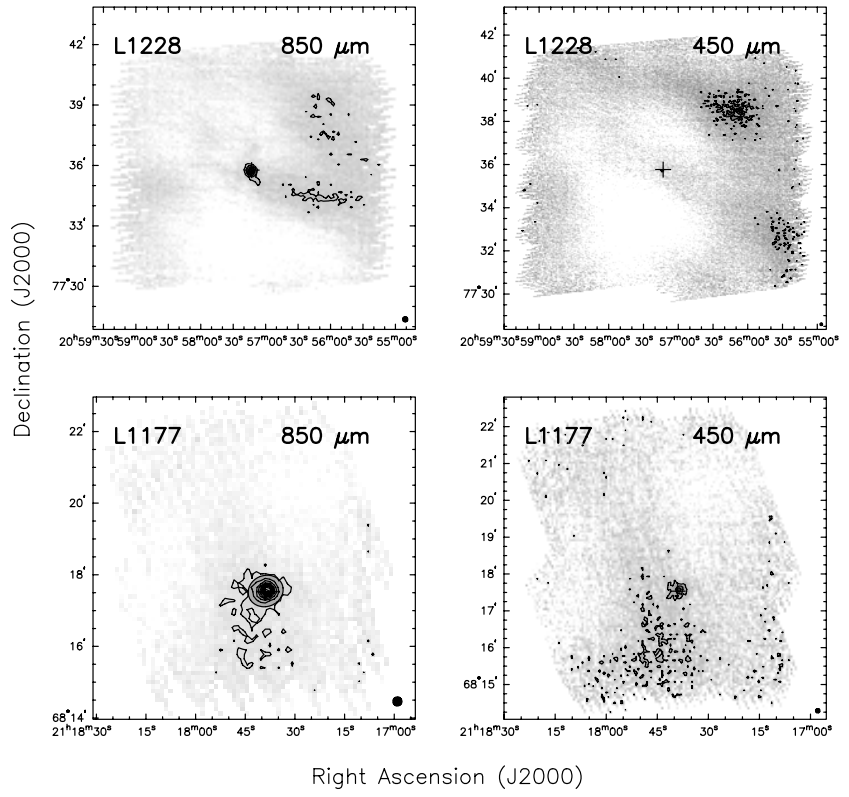

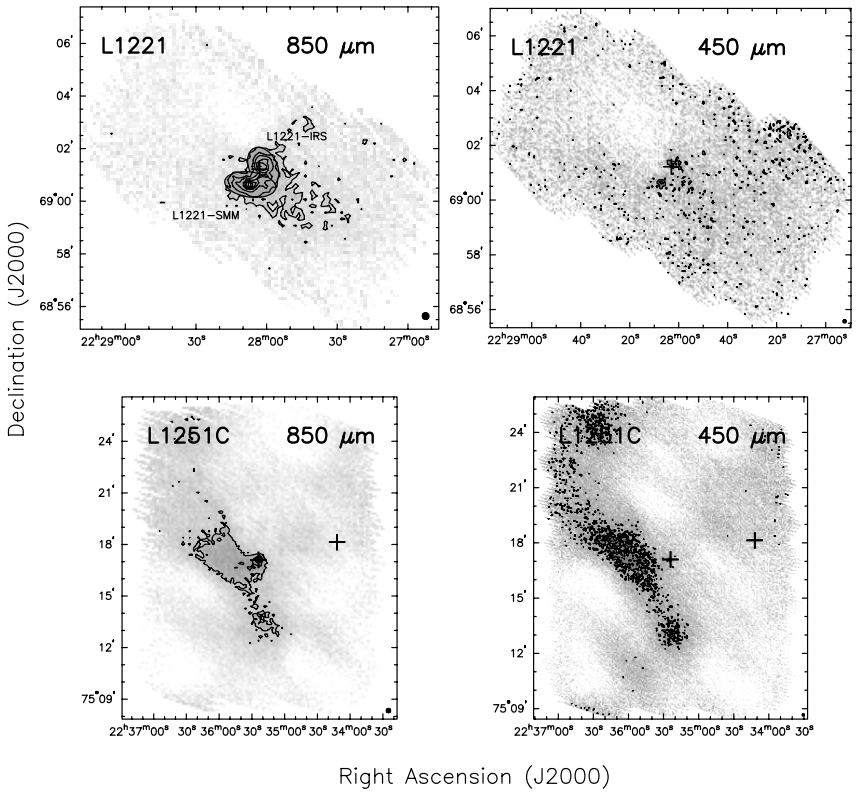

FIG. 1.—*Continued*

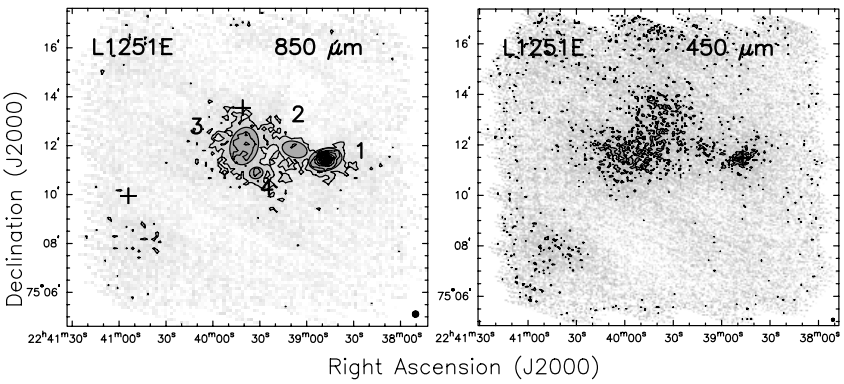

FIG. 1.—*Continued*

TABLE 3
SOURCE PROPERTIES AT 3 σ CONTOURS

Source	R.A. (J2000.0)	Decl. (J2000.0)	Major Axis (arcsec)	Minor Axis (arcsec)	Aspect Ratio	S_ν[a] (Jy)	$M_{\rm core}$[b] ($M_\odot$)
Per 4-B*	03 29 17.2	31 27 53	22	13	1.6	0.3 (0.1)	0.2 (0.1)
Per 4-C*	03 29 18.2	31 25 14	29	20	1.5	0.5 (0.2)	0.3 (0.1)
Per 4-A*	03 29 25.3	31 28 20	17	17	1	0.3 (0.1)	0.2 (0.1)
Per 5*	03 29 51.8	31 39 11	80	54	1.5	2.4 (0.7)	1.3 (0.4)
2MASS 0347392	03 47 39.4	31 19 08	27	18	1.5	0.2 (0.1)	0.1 (0.03)
IRAM 04191+1522*	04 21 56.8	15 29 51	75	46	1.6	1.4 (0.4)	0.2 (0.1)
IRAS 04191+1523*	04 22 00.6	15 30 26	38	30	1.2	0.6 (0.2)	0.1 (0.03)
L1521F*	04 28 39.7	26 51 51	142	87	1.6	5.9 (1.8)	1.0 (0.3)
L1524-4*	04 30 03.0	24 26 39	9	9	1	0.1 (0.03)	0.02 (0.01)
B18-1*	04 31 55.8	24 32 35	104	82	1.3	4.1 (1.2)	0.7 (0.2)
IRAS 04361+2547	04 39 14.0	25 53 23	34	27	1.2	0.7 (0.2)	0.1 (0.04)
RNO 43	05 32 19.4	12 49 41	43	38	1.1	1.8 (0.5)	2.6 (0.8)
B35A*	05 44 31.1	09 09 04	119	95	1.3	8.3 (2.5)	12.0 (3.6)
L43-IRS*	16 34 30.1	−15 46 59	55	33	1.7	1.8 (0.5)	0.3 (0.1)
L43-SMM*	16 34 35.8	−15 47 07	123	58	2.1	5.7 (1.7)	0.8 (0.2)
CB 68*	16 57 19.6	−16 09 20	68	51	1.3	3.9 (1.2)	0.5 (0.2)
L492*	18 15 47.8	−03 45 51	39	22	1.8	0.4 (0.1)	0.3 (0.1)
L723*	19 17 53.7	19 12 19	32	27	1.2	1.5 (0.5)	1.2 (0.4)
L1152*	20 35 44.3	67 52 52	38	21	1.8	1 (0.3)	1.0 (0.3)
CB 224	20 36 18.5	63 53 16	51	42	1.2	1 (0.3)	1.4 (0.4)
L1157-IRS	20 39 06.3	68 02 14	52	48	1.1	3 (0.9)	2.9 (0.9)
L1157-SMM	20 39 09.7	68 01 26	95	33	2.9	2.1 (0.6)	2.0 (0.6)
L1082C	20 51 28.2	60 18 38	50	45	1.1	1.3 (0.4)	1.9 (0.6)
L1082A-2	20 53 13.7	60 14 42	26	22	1.2	0.5 (0.2)	0.7 (0.3)
L1082A-1	20 53 27.6	60 14 34	38	28	1.3	1.1 (0.3)	1.6 (0.6)
L1082A-3	20 53 50.2	60 09 47	27	21	1.3	0.5 (0.2)	0.7 (0.3)
L1228*	20 57 13.4	77 35 43	34	29	1.2	2 (0.6)	0.7 (0.2)
L1177	21 17 38.8	68 17 33	59	52	1.1	3.1 (0.9)	2.3 (0.7)
L1251C[c]	22 35 24.6	75 17 04	35	31	1.1	2.2 (0.7)	1.8 (0.5)
L1221-IRS*	22 28 01.4	69 01 18	95	63	1.5	4.7 (1.4)	2.6 (0.8)
L1221-SMM*	22 28 06.9	69 00 38	117	57	2.1	4.7 (1.4)	2.6 (0.8)
L1251E-1*	22 38 48.1	75 11 26	83	55	1.5	6.4 (1.9)	5.2 (1.6)
L1251E-2*	22 39 07.7	75 11 51	62	39	1.6	1.9 (0.6)	1.5 (0.5)
L1251E-4*	22 39 32.3	75 10 53	33	28	1.2	0.9 (0.3)	0.7 (0.2)
L1251E-3*	22 39 40.0	75 11 59	93	68	1.4	5.2 (1.6)	4.2 (1.3)

NOTES.—Asterisks indicate cores observed in the c2d program. Units of right ascension are hours, minutes, and seconds, and units of declination are degrees, arcminutes, and arcseconds.

[a] We give the 850 μm flux calculated for the elliptical aperture described in this table.

[b] The mass of the core is derived from the 850 μm flux assuming an isothermal temperature of 15 K.

[c] As discussed in the text, the properties of L1251C were calculated with the analysis threshold set to 5 σ.

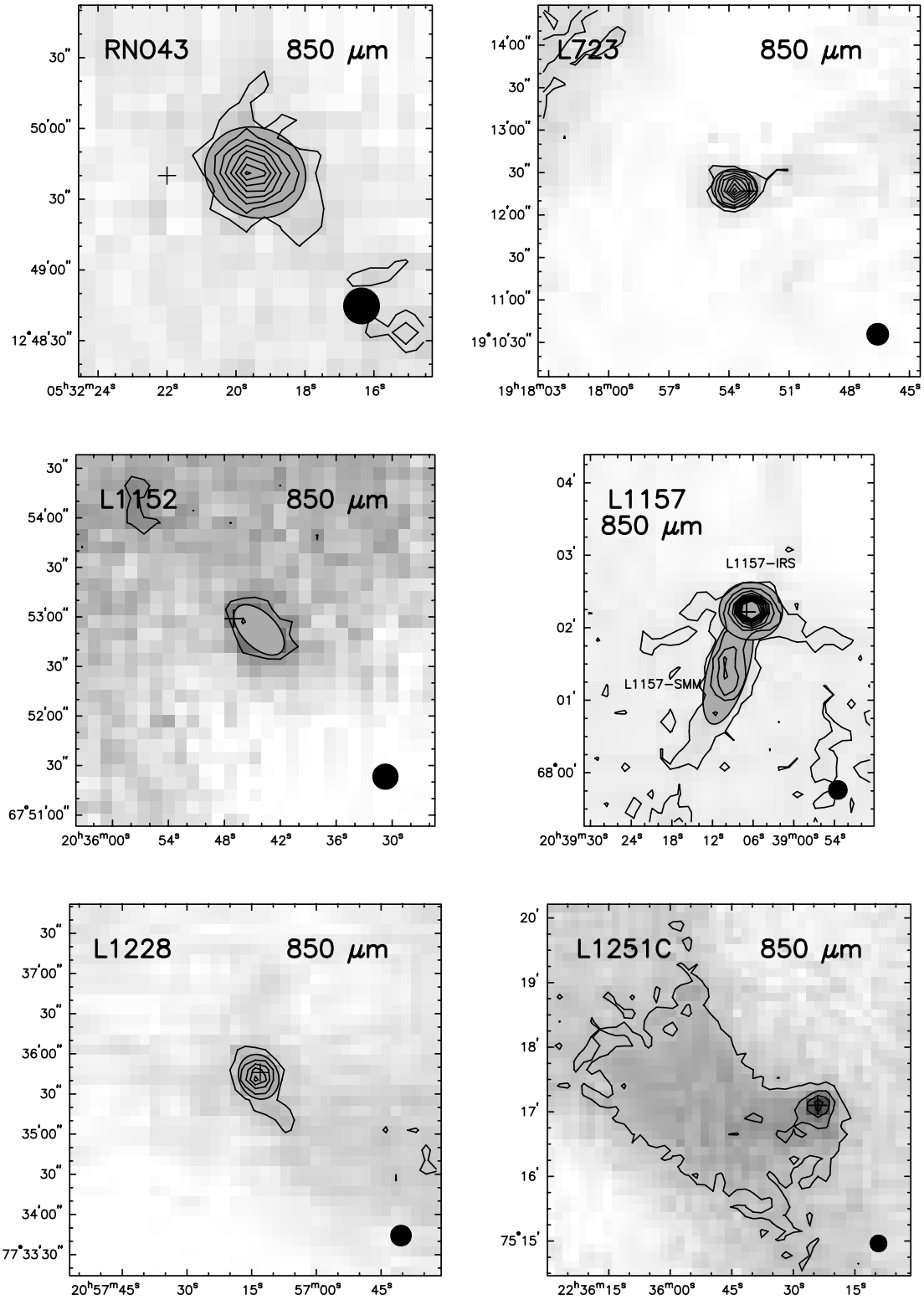

FIG. 2.—Central regions of the maps that cover especially large regions. The ellipses and crosses are the same as in Fig. 1.

3 σ). At this point, we examined each rebinned, dual-beam map to search for evidence of bad data, such as stripes or other artifacts, missed during the despiking and cleaning tasks.

The rebinned maps are the telescope's dual-beam function convolved with the sky. We used *remdbm* to remove the dual-beam signature from the map. This package uses the Emerson2 (Emerson 1995; Emerson et al. 1979) technique to deconvolve the data and create the single-beam map of the source. We used no high-frequency filtering. We assessed the rms noise of the map with Starlink's *stats* package and created the maps in Figure 1. The contours begin at 2 σ and increase by 2 σ; the gray scale begins at -2 σ and increases to the image maximum. Crosses mark the positions of *IRAS* sources, which were selected using the criteria of Lee & Myers (1999).

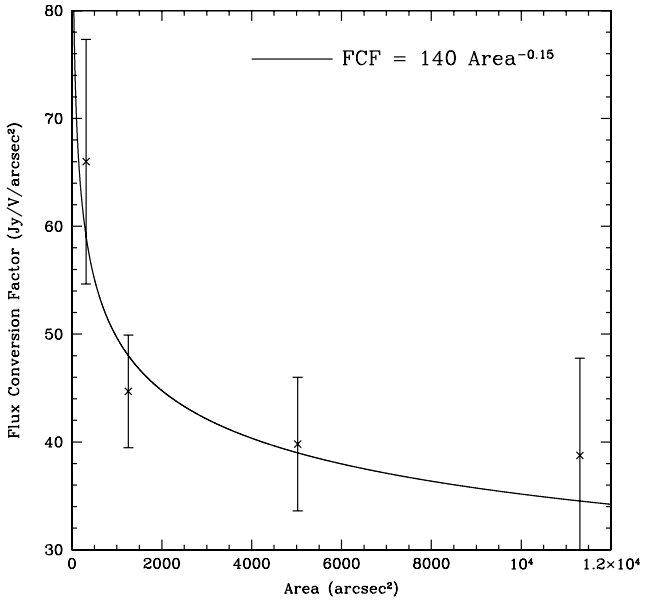

FIG. 3.—Data for FCFs (*crosses*) fitted with a function in order to calculate the FCFs for apertures with different areas. This function ($FCF = 140 \times area^{-0.15}$) is used in calculating the FCFs used to determine the source fluxes in Table 3.

We used Starlink's Extractor, which is based on SExtractor (Bertin & Arnouts 1996), to extract source information for each of the maps in Figure 1 (Chipperfield & Draper 2004). This includes the source positions (barycenter), major and minor axes, and aspect ratios in Table 3. The aspect ratio is the ratio of major-to-minor axes as measured at the 3 σ threshold limit, except for L1251C, for which we used a threshold limit of 5 σ. For L1251C, the 3 σ limit extracted a source that was much larger than the obviously compact and embedded core. In Figure 1 we have overlaid on the maps an ellipse that matches the extracted source by Extractor. For those observations with especially large fields, maps covering just the central regions are shown in Figure 2.

2.4. *Calibration*

In Table 2 we list flux conversion factors (FCFs) for all calibrators observed during the course of this project. To calculate the FCF, we divide the flux of the calibrator, which is assumed to be a point source, by the total data counts (i.e., volts) in a given aperture. To determine the FCF for a 20″ aperture, for example, we divide the flux of the calibrator by the total data counts for a 20″ aperture, which gives the FCF in units of janskys per volt. Then we use this FCF to convert the data counts for the cores into flux units (for a 20″ aperture). This method of calibration has

TABLE 4
SOURCE FLUXES

Source Name	S_{20}^{850}[a]	S_{40}^{850}	S_{80}^{850}	S_{120}^{850}	S_{20}^{450}	S_{40}^{450}
Per 4-B*	0.5 (0.09)	0.7 (0.1)	0.9 (0.2)	0.6 (0.3)	2.0 (1.1)	2.8 (1.6)
Per 4-C*	0.4 (0.08)	0.9 (0.1)	1.4 (0.3)	2.0 (0.5)	2.1 (1.1)	4.4 (2.4)
Per 4-A*	0.3 (0.05)	0.6 (0.1)	0.9 (0.2)	0.9 (0.3)	3.3 (1.7)	7.7 (4.2)
Per 5*	0.8 (0.14)	1.3 (0.2)	3.0 (0.5)	4.9 (1.2)	5.6 (2.9)	11.9 (6.4)
2MASS 0347392	0.2 (0.04)	0.5 (0.1)	0.9 (0.2)	1.1 (0.3)	...	...
IRAM 04191+1522*	0.5 (0.09)	0.9 (0.1)	1.8 (0.3)	2.8 (0.7)	1.6 (0.8)	1.1 (0.7)
IRAS 04191+1523*	0.4 (0.07)	0.6 (0.1)	1.2 (0.2)	1.9 (0.5)	1.4 (0.7)	1.4 (0.8)
L1521F*	0.6 (0.10)	1.5 (0.2)	4.2 (0.7)	6.8 (1.6)	4.6 (2.4)	13.3 (7.2)
L1524-4*	0.3 (0.05)	0.6 (0.1)	1.9 (0.3)	3.8 (0.9)	2.0 (1.0)	5.6 (3.0)
B18-1*	0.3 (0.04)	1.1 (0.1)	3.4 (0.6)	6.1 (1.5)	9.1 (4.6)	22.8 (12.3)
IRAS 04361+2547	0.5 (0.08)	0.8 (0.1)	1.5 (0.3)	1.9 (0.5)	...[b]	...
RNO 43	1.2 (0.2)	1.7 (0.3)	2.3 (0.5)	2.7 (0.7)	8.8 (4.4)	13.8 (7.5)
B35A*	0.8 (0.13)	2.6 (0.3)	6.7 (1.1)	10.0 (2.4)	3.5 (1.7)	12.2 (6.6)
L43-IRS*	0.6 (0.10)	1.4 (0.2)	2.9 (0.5)	4.8 (1.2)	5.9 (3.0)	15.0 (8.1)
L43-SMM*	0.7 (0.11)	2.0 (0.2)	5.2 (0.8)	8.2 (2.0)	...	...
CB 68*	1.1 (0.17)	2.3 (0.3)	5.5 (0.9)	9.4 (2.3)	10.8 (5.4)	27.8 (14.9)
L492*	0.2 (0.03)	0.5 (0.1)	1.4 (0.2)	2.1 (0.5)	0.7 (0.3)	1.7 (0.9)
L723*	1.4 (0.26)	1.4 (0.3)	1.2 (0.4)	0.3 (0.4)	4.0 (2.1)	0.7 (0.9)
L1152*	0.5 (0.08)	1.2 (0.2)	2.2 (0.4)	2.9 (0.7)	2.9 (1.4)	8.3 (4.4)
CB 224	0.4 (0.07)	0.8 (0.1)	1.5 (0.3)	1.9 (0.5)	2.3 (1.2)	2.8 (1.6)
L1157-SMM	0.7 (0.11)	1.2 (0.2)	2.5 (0.4)	5.7 (1.4)	...	...
L1157-IRS	2.2 (0.39)	2.5 (0.5)	3.7 (0.8)	5.0 (1.3)	9.7 (4.9)	13.2 (7.2)
L1082C	0.3 (0.05)	1.0 (0.1)	2.2 (0.4)	3.4 (0.8)	1.9 (1.0)	4.8 (2.6)
L1082A-2	0.4 (0.07)	0.6 (0.1)	0.8 (0.2)	0.5 (0.2)	...	...
L1082A-1	0.8 (0.15)	1.1 (0.2)	1.5 (0.3)	1.7 (0.5)	1.1 (0.6)	0.02 (0.4)
L1082A-3	0.5 (0.08)	0.6 (0.1)	1.1 (0.2)	1.7 (0.4)	1.7 (0.9)	1.8 (1.0)
L1228	1.2 (0.20)	2.0 (0.3)	3.5 (0.7)	4.5 (1.2)	3.6 (2.1)	1.1 (1.4)
L1177	1.6 (0.29)	2.4 (0.4)	3.9 (0.7)	5.3 (1.3)	6.3 (3.2)	10.7 (5.8)
L1251C	0.9 (0.2)	2.3 (0.3)	5.2 (0.9)	8.7 (2.1)	8.9 (4.5)	16.4 (8.9)
L1221-IRS*	1.0 (0.16)	2.0 (0.2)	4.9 (0.8)	8.1 (2.0)	4.9 (2.5)	10.4 (5.6)
L1221-SMM*	1.2 (0.19)	2.0 (0.3)	4.5 (0.8)	7.9 (1.9)	6.5 (3.3)	11.3 (6.1)
L1251E-1*	2.0 (0.33)	4.0 (0.5)	7.0 (1.3)	9.5 (2.3)	24.1 (12.1)	49.5 (26.6)
L1251E-2*	0.5 (0.08)	1.4 (0.2)	3.5 (0.6)	5.9 (1.4)	...	...
L1251E-4*	0.6 (0.10)	1.2 (0.2)	3.3 (0.5)	6.6 (1.6)	...	...
L1251E-3*	0.5 (0.09)	1.9 (0.2)	5.2 (0.8)	9.4 (2.2)	...	...

NOTE.—Asterisks indicate cores observed in the c2d program.

[a] The flux in janskys for a 20″ aperture. The remaining columns are fluxes in 40″, 80″, and 120″ apertures. We also give the 450 μm fluxes as measured in 20″ and 40″ apertures.

[b] We require at least a 2 σ detection to report the flux measurement; several cores did not satisfy this requirement in the 450 μm data.

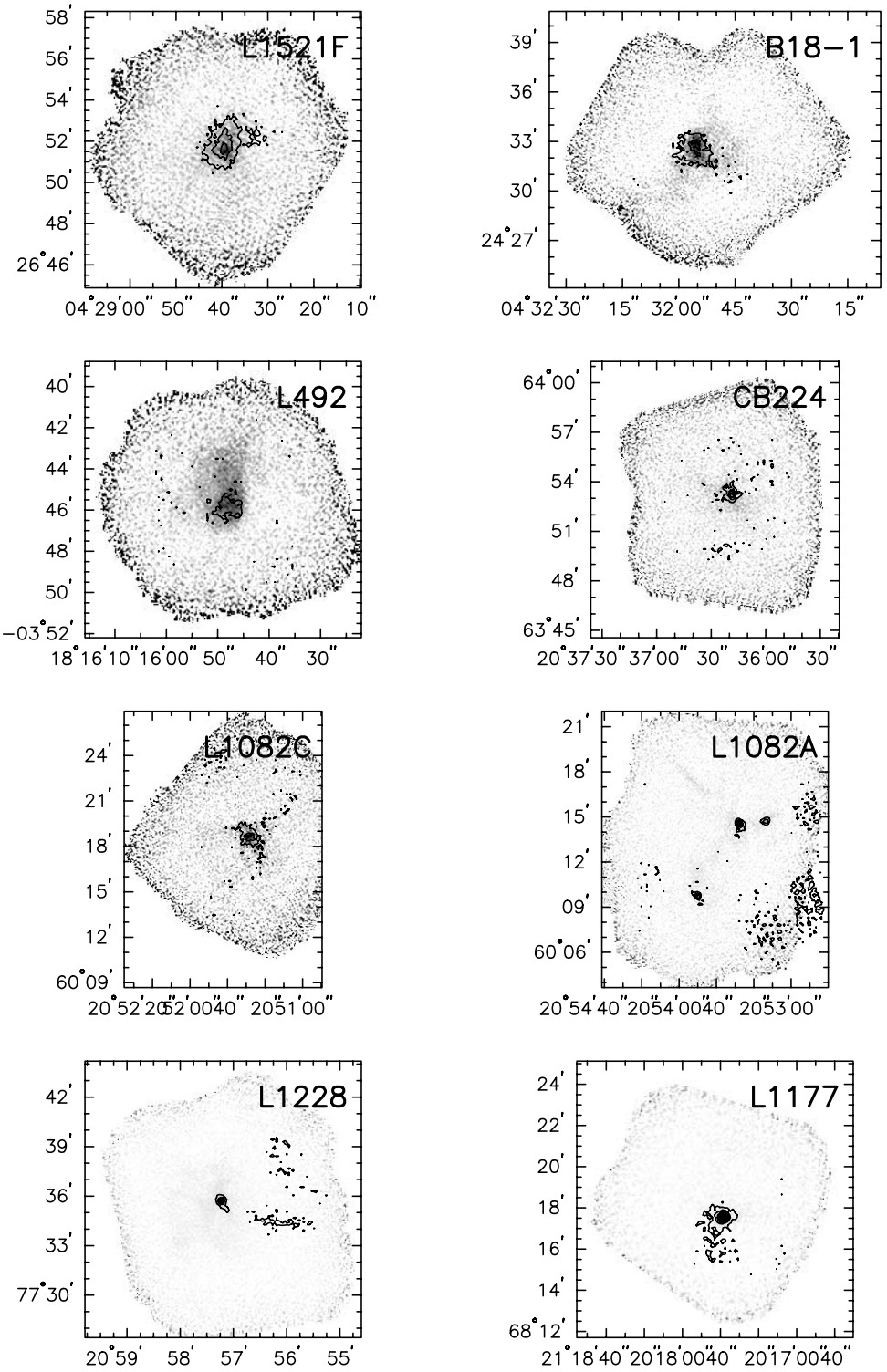

FIG. 4.—MAMBO data for cores (*gray scale*; J. Kauffmann 2006, in preparation). The contours represent 850 μm observations, as shown in Fig. 1. The SCUBA and MAMBO data show good agreement on these cores.

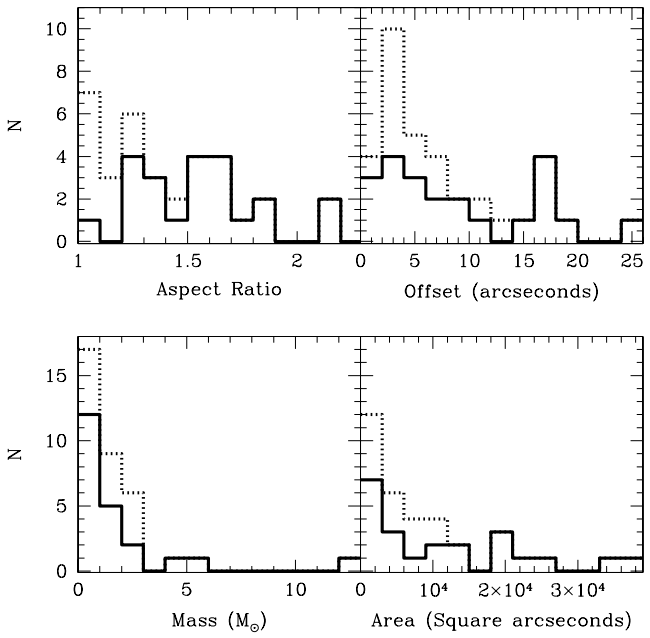

FIG. 5.—Isothermal masses, aspect ratios, and areas, as reported in Table 3. The solid line represents the data for cores observed by c2d; the dotted line shows the histogram for all cores presented in this paper. The area is calculated as πab, the area of an ellipse. The top right panel shows the difference in position of the peak pixel and the barycenter position.

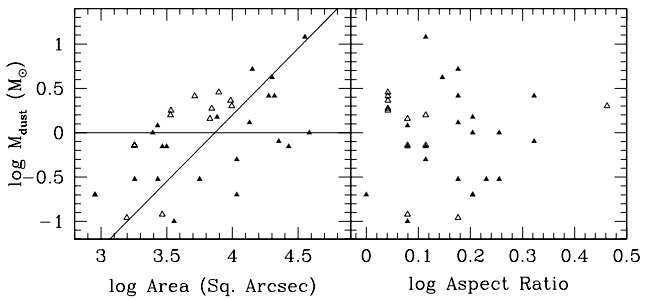

FIG. 6.—Mass of each core vs. size and aspect ratio as measured at the 3 σ level. The filled triangles represent cores observed by c2d; the open triangles represent cores not observed by c2d. To calculate the dust mass, we use the flux in the elliptical aperture (as shown in Fig. 1) and assume an isothermal temperature of 15 K. The lines in the left panel represent what is expected for this relationship in cores with constant column density (flat) and constant density ($M \propto \text{area}^{1.5}$).

been used by a number of authors (e.g., Shirley et al. 2000; Young et al. 2003) and is superior to using beam-sized apertures because of the significant and variable sidelobes on the JCMT's beam at 850 and 450 μm. These sidelobes, at 850 μm, can extend to 50″ even though the beam size is $\sim$15″ (Shirley et al. 2000).

In using the FCF, we simply average all values, except those for Jupiter and IRC 10216, and give this average and standard deviation in Table 2. As suggested on the SCUBA Web site,[2] we do not use Jupiter and IRC 10216 for flux calibration. We do not use FCFs when the uncertainty approaches 100%, as for the 450 μm FCFs for 80″ and 120″ apertures, but we list them in Table 2 along with all of the average calibration factors.

In Table 2 we also give the FWHM of a Gaussian fit to the JCMT beam pattern at 850 μm. We fit a Gaussian to the observed intensity profile with Starlink's *psf* routine (setting `gauss=True`) and deconvolve the measured beam size for the planet diameter (Uranus and Mars have semidiameters of 1.″72 and 3.″67, respectively). The average FWHM of the beam over all nights was 15.″5 $\pm$ 0.″5. The nominal beam at 450 μm is about 8″, but it can be as large as 11″ (Young et al. 2003). Because the quality of the 450 μm data is poor, we do not calculate the 450 μm beam profile for these observations.

We have calculated fluxes for each source whose size and shape were determined by Extractor. To determine the FCFs for these noncircular apertures, we have fit a function to the FCFs of the circular apertures. Because the sidelobes contribute significantly to the aperture sums, the FCF decreases as the area of the aperture increases. In Figure 3 we show the average FCFs for the 20″, 40″, 80″, and 120″ apertures; the solid line indicates a fit to these data: FCF $= 140 \times \text{area}^{-0.15}$, where "area" is the area of the aperture in square arcseconds. For the noncircular apertures, we calculate the area (πab) and determine the FCFs from the above relationship. Then we calculate the flux and ascribe a 30% uncertainty to this measurement, which is a liberal estimate of the flux uncertainty at 850 μm. The fluxes in the elliptical apertures are given in Table 3, and the fluxes in the fixed circular apertures of different diameters are given in Table 4. The apertures are those agreed to for papers presenting ancillary data to the c2d project. These ancillary continuum data are in preparation for publication and include observations of the c2d cores from the Max-Planck-Millimeter-Bolometer (MAMBO; Kreysa et al. 1998), the Submillimeter High Angular Resolution Camera II (Dowell et al. 2003), and the Sest Imaging Bolometer Array (Nyman et al. 2001). In Figure 4 we show the MAMBO data in gray scale with the SCUBA 850 μm observations represented by contours, as in Figure 1. There is good agreement between these sets of data in representing the detected continuum emission.

Kirk et al. (2005) observed two of these sources with SCUBA. For L1521F, they measured the fluxes in a 150″ aperture: 3.23 $\pm$ 0.23 Jy at 850 μm and 12.4 $\pm$ 2.4 Jy at 450 μm. These are compared to our measurements of 4.2 $\pm$ 0.7 Jy at 850 μm (120″ aperture) and 13.3 $\pm$ 7.2 Jy at 450 μm (40″ aperture). For L43, Kirk et al. (2005) measured 5.4 $\pm$ 0.23 and 28.6 $\pm$ 1.8 Jy (at 850 and 450 μm), which compares to our measured values of 4.8 $\pm$ 1.2 and 15.0 $\pm$ 8.1 Jy.

3. RESULTS

In this section we give the basic results for these observations: maps, fluxes, and characteristics of the cores. Further analysis of these data will follow in later papers and will include *Spitzer* observations and other ancillary data (near-infrared, millimeter, etc.).

Of the 38 cores observed with SCUBA, 13 were not detected at either 850 or 450 μm. For these cores and the detected objects, we list the 3 σ noise level in Table 1, starting with source Per 7A. These cores do not appear in the other tables. The maps for the detected cores are shown in Figure 1. For those observations with especially large fields, maps covering just the central regions are shown in Figure 2. In both of these figures, the crosses represent *IRAS* sources selected by the criteria of Lee & Myers (1999), and the ellipses represent the sources chosen by Extractor.

3.1. *Size, Shape, and Mass*

In Table 3 we give the size and aspect ratio of each core as measured at the 3 σ level with Extractor. We also list the 850 μm flux within the aperture described by this size and aspect ratio;

[2] See http://www.jach.hawaii.edu/JCMT/continuum/calibration/sens/secondary_2004.html.

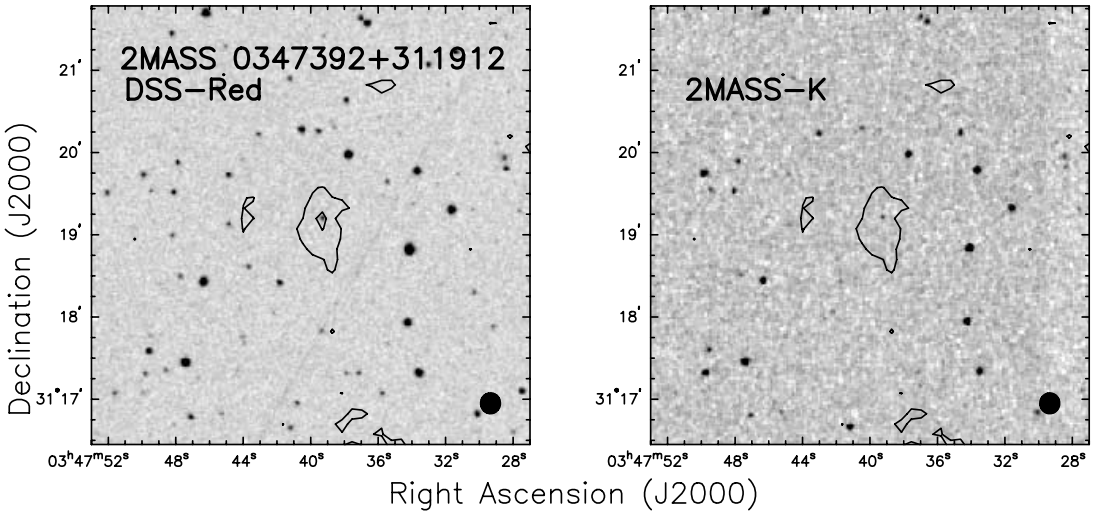

FIG. 7.—Data for 2MASS 0347392+311912. The gray scale in the left panel is from the DSS, and the right panel shows the 2MASS *K*-band image. The contours are from the SCUBA 850 μm observations. Contours begin at 2 σ and increase by 2 σ; we do not draw the 4 σ contour in the right panel because it obscures the 2MASS source.

the isothermal mass of each core is derived from that 850 μm flux, assuming a temperature of 15 K (see eq. [2] in Young et al. 2003); the dust opacity used in these calculations is $\kappa_\nu = 0.018$ cm^2 g^{-1} (for OH5 dust; Ossenkopf & Henning 1994). The assumed temperature is relevant; a variation from 10 to 20 K in isothermal temperature causes an increase in the mass by a factor of 3.3. The sizes are, with one exception, much larger than the beam, so deconvolution of the beam is unnecessary. The very compact core is not included in the plots.

In Figure 5 we plot histograms of the isothermal masses, aspect ratios, and core areas as reported in Table 3. The difference in the position of the peak pixel and the barycenter position (i.e., the center of the fitted ellipse) is also shown as a histogram in this figure; this is a measure of axisymmetry. The core area is equal to πab, the area of an ellipse. In order to maintain consistency with other c2d ancillary data papers to come, we show the data for only those cores observed in the c2d program (i.e., the objects with asterisks in Table 3). The dotted lines represent the histogram for the entire sample of cores.

In Figure 6 we plot the core mass versus the size and aspect ratio of the cores (as measured at the 3 σ level); the data for those cores observed in the c2d program are represented by filled triangles, and the cores not observed by c2d are shown as open triangles. The lines in the left panel (with area) represent what is expected for this relationship in cores with constant column density (flat) and constant density ($M \propto \mathrm{area}^{1.5}$).

The dust mass increases with size, as one might expect, although the scatter is large. There are also a number of cores that have low masses despite their large core size. Perhaps these objects are cold, starless cores.

3.2. *Multiplicity*

Several of the maps contain more than one dense core: IRAM 04191+1522, L1082A, L1157, L1221, L1251E, L43, and Per 4. Three other objects have some extended emission, which is either real or an artifact of the double-beam deconvolution (Pierce-Price 2002): B35A, CB 68, and L1251C. For B35A, at least, the extended emission does appear to be real, because the N_2H^+ map shows similar structure (Caselli et al. 2002). The N_2H^+ map of L1251C is also similar to the 850 μm continuum image. CB 68 was mapped by Huard et al. (1999), and their map, while much smaller and more sensitive than ours, does not appear to show the extended emission in Figure 1.

In all but one case, only one object in each of the multiple core systems was detected by *IRAS*. This implies that either these multiple cores are at different stages of evolution or that some of the cores are forming objects with lower masses than their companions and hence are not detected by *IRAS*. With *Spitzer* we have begun to unravel the mystery of these cores. For example, IRAM 04191+1522 does harbor an infrared source detected with IRAC and MIPS (Dunham et al. 2006), but L43-SMM does not appear to harbor an embedded source down to very low luminosities (T. L. Huard et al. 2006, in preparation).

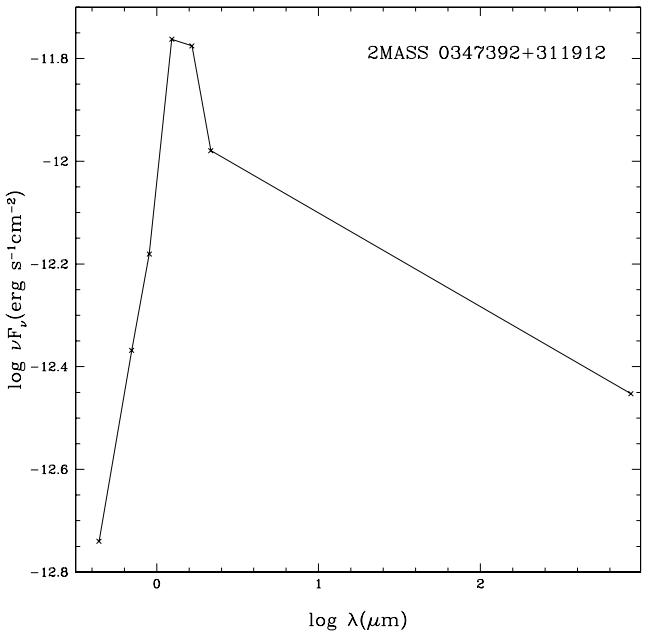

FIG. 8.—SED for 2MASS 0347392+311912. The *B*, *R*, and *I* fluxes are from the USNO-B1.0 catalog; *J*, *H*, and *K* data are from 2MASS. The 850 μm data are from this paper.

4. 2MASS 0347392+311912

We inadvertently observed 2MASS 0347392+311912, having intended to observe a known core in Perseus instead. The source lies outside of the c2d observations for Perseus, so we have no mid- or far-infrared data. The 2MASS source, however, did have detectable submillimeter emission at 850 μm (0.2 Jy).

In Figure 7 we show the 850 μm data overlaid on 2MASS *K*-band and Digitized Sky Survey *R*-band images. In both the near-infrared and optical maps, the source appears pointlike and is clearly detected. In Figure 8 we plot the SED for this source, including the near-infrared data from 2MASS and *B*, *R*, and *I* measurements from the USNO-B1.0 catalog. The SED peaks at 1.65 μm (*H*) but has substantial submillimeter emission (0.1 Jy at 850 μm). This source may be a previously unknown protostar and is possibly near the Perseus molecular cloud.

5. SUMMARY

We have presented SCUBA observations of low-mass cores that were initially proposed to be observed with the *Spitzer Space Telescope* as a part of the c2d Legacy program. We describe these observations and the data reduction and analysis. In addition, we show the maps, source fluxes, and source sizes. The core mass has been calculated from the 850 μm fluxes, and we analyze how the mass varies with source size and shape. We find several small clouds with multiple distinct cores, but for most regions only one of the cores is detected by *IRAS*. Finally, we present inadvertent observations of an object near Perseus that may be a newly discovered protostar. All data presented here are publicly available as FITS images.[3]

The authors acknowledge the data analysis facilities provided by the Starlink Project, which is run by CCLRC on behalf of PPARC. We are also grateful to JCMT support scientists Remo Tilanus, Vicky Barnard, and Douglas Pierce-Price for much needed help in observing and data reduction. Support for this work, part of the *Spitzer* Legacy Science Program, was provided by NASA through contract 1224608 issued by the Jet Propulsion Laboratory, California Institute of Technology, under NASA contract 1407. Astrochemistry in Leiden is supported by a NWO Spinoza grant and a NOVA grant. This work was also supported by NASA grants NAG5-10488 and NNG04GG24G.

[3] See http://peggysue.as.utexas.edu/SIRTF/DATA/.

REFERENCES

Benson, P. J., & Myers, P. C. 1989, ApJS, 71, 89
Bertin, E., & Arnouts, S. 1996, A&AS, 117, 393
Caselli, P., Benson, P. J., Myers, P. C., & Tafalla, M. 2002, ApJ, 572, 238
Chipperfield, A. J., & Draper, P. W. 2004, Extractor: An Astronomical Source Detection Program (Starlink User Note 226.8; http://www.starlink.rl.ac.uk/star/docs/sun216.htx/sun216.html)
de Geus, E. J., de Zeeuw, P. T., & Lub, J. 1989, A&A, 216, 44
Dobashi, K., Bernard, J.-P., Yonekura, Y., & Fukui, Y. 1994, ApJS, 95, 419
Dowell, C. D., et al. 2003, Proc. SPIE, 4855, 73
Dunham, M. M., et al. 2006, ApJ, in press
Elias, J. H. 1978, ApJ, 224, 857
Emerson, D. T. 1995, in ASP Conf. Ser. 75, Multi-Feed Systems for Radio Telescopes, ed. D. T. Emerson & J. M. Payne (San Francisco: ASP), 309
Emerson, D. T., Klein, U., & Haslam, C. G. T. 1979, A&A, 76, 92
Enoch, M. L., et al. 2006, ApJ, 638, 293
Evans, N. J., II, et al. 2003, PASP, 115, 965
Goldsmith, P. F., Snell, R. L., Hemeon-Heyer, M., & Langer, W. D. 1984, ApJ, 286, 599
Holland, W. S., et al. 1999, MNRAS, 303, 659
Huard, T. L., Sandell, G., & Weintraub, D. A. 1999, ApJ, 526, 833
Jenness, T., & Lightfoot, J. F. 1997, SURF: SCUBA User Reduction Facility ver. 1.5-1 User's Manual (Hilo: Joint Astron. Cent.), http://www.starlink.rl.ac.uk/star/docs/sun216.htx/sun216.html
Jijina, J., Myers, P. C., & Adams, F. C. 1999, ApJS, 125, 161
Johnstone, D., Di Francesco, J., & Kirk, H. 2004, ApJ, 611, L45
Jørgensen, J. K., et al. 2006, ApJ, 645, 1246
Kirk, J. M., Ward-Thompson, D., & André, P. 2005, MNRAS, 360, 1506
Kreysa, E., et al. 1998, Proc. SPIE, 3357, 319
Kun, M. 1998, ApJS, 115, 59
Kun, M., & Prusti, T. 1993, A&A, 272, 235
Lee, C. W., & Myers, P. C. 1999, ApJS, 123, 233
Lee, C. W., Myers, P. C., & Tafalla, M. 2001, ApJS, 136, 703
Motte, F., André, P., & Neri, R. 1998, A&A, 336, 150
Murdin, P., & Penston, M. V. 1977, MNRAS, 181, 657
Nyman, L., et al. 2001, Messenger, 106, 40
Ogura, K., & Sugitani, K. 1998, Publ. Astron. Soc. Australia, 15, 91
Ossenkopf, V., & Henning, T. 1994, A&A, 291, 943
Pierce-Price, D. P. I. 2002, Ph.D. thesis, Cambridge Univ.
Shirley, Y. L., Evans, N. J., II, Rawlings, J. M. C., & Gregersen, E. M. 2000, ApJS, 131, 249
Straizys, V., Cernis, K., & Bartasiute, S. 2003, A&A, 405, 585
Straizys, V., Cernis, K., Kazlauskas, A., & Meistas, E. 1992, Baltic Astron., 1, 149
Visser, A. E., Richer, J. S., & Chandler, C. J. 2002, AJ, 124, 2756
Woermann, B., Gaylard, M. J., & Otrupcek, R. 2001, MNRAS, 325, 1213
Yonekura, Y., Dobashi, K., Mizuno, A., Ogawa, H., & Fukui, Y. 1997, ApJS, 110, 21
Young, C. H., Shirley, Y. L., Evans, N. J., II, & Rawlings, J. M. C. 2003, ApJS, 145, 111